A study on slab-wooden dust-slab phantom for the development of thorax phantom

Swati Dubey[1], Priyusha Bagdare[1]*, Sanjay Kumar Ghosh[1], Om Prakash Gurjar[2], Virendra Bhandari[2], Krishna Lal Gupta[2], Saurabh Karnawat[2]

1. School of Studies in Physics, Vikram University, Ujjain (M.P.) 456001
2. Roentgen-SAIMS Radiation Oncology Centre, Sri Aurobindo Institute of Medical Sciences, Indore, Madhya Pradesh - 453111, India

A R T I C L E I N F O	A B S T R A C T
Article type: Original Article **Article history:** Received: Jun 12, 2017 Accepted: Nov 28, 2017 **Keywords:** Hounsfield Number Quality Assurance SP34 Slab Phantom Thorax Phantom	***Introduction***: The determination of accurate dose distribution is an issue of fundamental importance in radiotherapy, especially with regard to the fact that the human body is a heterogeneous medium. Therefore, the present study aimed to analyze the density and isodose depth profiles of 6 MV beam in a SP34 slab-wooden dust (pine)-SP34 slab (SWS) heterogeneous phantom. ***Materials and Methods:*** The density of SP34 slab, wooden dust of pine, and thoracic region of 10 patients were calculated using computed tomography (CT) images. The depths of isodose lines were measured for 6 MV beam on the CT images of the chest, SP34 slab phantom, and SWS phantom. Dose calculation was performed at the depths of 2, 13, and 21 cm in both phantoms. Furthermore, patient-specific quality assurance (QA) was implemented using both phantoms. ***Results:*** The mean densities of the lung, SP34 slabs, and wooden dust were 0.29, 0.99, and 0.27 gm/cc respectively. The mean depths of different isodose lines in the SWS phantom were found to be equivalent to those in actual patients. Furthermore, the percentage variation between the planned and measured doses was higher in the SWS phantom as compared to that in the SP34 phantom. Furthermore, the percentage variation between the planned and measured doses in patient-specific QA was higher in the SWS phantom as compared to that in the SP34 phantom. ***Conclusion:*** As the findings indicated, the density and isodose depth profiles of the SWS phantom were equivalent to those of the actual thoracic region of human.

Introduction

The interaction of photon with materials of different densities has a great importance in radiation field. It is well-established that photon of particular energy deposit dose differently inside the medium of various densities [1]. Human body is a heterogeneous medium having regions of different density (e.g., the bones, teeth, lung, air cavities, and tissues) and radiological behavior [2]. Therefore, the determination of accurate dose deposition in a heterogeneous medium plays a crucial role in the clinical outcome of radiotherapy [3].

Dose calculation algorithms play an important role in the accurate estimation of dose in the medium for treatment planning [4-5]. The algorithms, used in commercial treatment planning system (TPS), such as analytical anisotropic, collapsed cone convolution, and pencil beam convolution algorithms, have limitations in the calculation of accurate dose when complex geometry and tissue heterogeneities are involved [6-9]. The American Association of Physicists in Medicine (AAPM) and

Task Group 65 states that the achievement of accuracy of 2% in dose delivery is a challenging goal in cases with tissue inhomogeneities [10].

The employment of Monte Carlo (MC) algorithm would provide more accurate results when charged particle disequilibrium occurs near the air-tissue interface, such as the lung, brain, oral cavity, breast, and head-and-neck sites. Acuros XB (AXB) is one of the algorithms introduced with Eclipse TPS that is based on the MC code [11-13].

Not only do we need the algorithm for the calculation of dose inside any medium of interest, we also require to have the best dosimetric tools and practices to verify the accuracy of this measurement. According to the International Commission on Radiation Units and Measurements (ICRU) 83 (2010), the improvement of the dosimetric accuracy requires the promotion of the dosimetric equipment and procedure of patient-specific quality assurance (QA) [14].

The use of the tissue-equivalent phantoms is a common practice to verify the accuracy of dose

*Corresponding Author: Research Scholar, School of Studies in Physics , Vikram University, , Ujjain (M.P.) 456001 , India Tel: +91-8982142093; Email: priyushabagdare@gmail.com

distribution. Since nearly 65% of the human body consists of water [15], the phantoms are water equivalent as suggested by ICRU 83, Technical Reports Series 398, and AAPM Task Group Report 120. Based on these guidelines, the medium of reference for QA purpose is water or water equivalent phantoms having a uniform density [14, 16, 17]. The verification of the accuracy of the dose calculated by advanced algorithms requires the implementation of patient-specific QA on heterogeneous phantoms instead of water equivalent homogeneous phantoms [18]. The advancement in the recent diagnostic techniques has provided us with the knowledge that human body comprises of bone, fat, air cavities, and tissues of varied densities, which make it a complex heterogeneous medium [2].

The anthropomorphic phantoms that are used for dosimetry have their own limitations. For instance, they do not have the exact curvature, shape, and density pattern of the actual human body [19]. Accordingly, the phantom developed by T. Nishio *et al.* and Chang *et al.* needed an improvement to render long-term reproducible results [20, 21]. With this background in mind, the present study aimed to measure the density and isodepth dose profile of wooden dust for the development of a heterogeneous thorax phantom and verify patient-specific QA using homogeneous and heterogeneous phantoms.

Materials and Methods

Experimental tools and computed tomography

Computed tomography (CT) image sets with slice thickness of 3 mm were obtained from 10 patients, SP34 slab phantom, and SP34 slab-wooden dust (pine)-SP34 slab (SWS) phantom using Siemens SOMATOM Definition AS scanner (Siemens Medical Systems, Germany). The ionization chamber (0.13 cc; IBA Dosimetry, Germany) was placed inside the SP34 slab and SWS phantoms while taking CT images. Subsequently, all the CT images were imported to Eclipse TPS, version 8.9 (Varian Medical Systems, Palo Alto, CA).

The CT images of thoracic region in patient had three regions, including chest wall with the mean thickness of 3 cm, lung with the mean depth of 16 cm, and soft tissue region of 5 cm. The SWS phantom was designed by placing 3-cm SP34 slabs above a $20 \times 20 \times 20$ cm^3 wooden box filled with the wooden dust of pine and 5-cm SP34 slabs at the bottom as shown in Figure 1. The wall thickness of the wooden box was 0.5 cm.

Furthermore, the arrangement of SP34 slab phantom was accomplished using 20 slabs "solid phantom SP34" (IBA Dosimetry BmbH, Schwarzenbruck, Germany) made up of polystyrene C_8H_8 (composition: 98% polystyrene + 2% TiO_2) with the thickness of 1 cm, effective atomic number of 5.74, and area of 30×30 cm^2 with a uniform density.
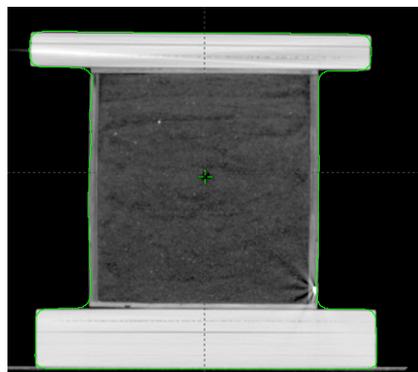

Figure 1. Schematic representation of WDAS phantom

Density Measurement

The density of slab, wooden dust, chest wall, lung, and soft tissue was calculated using the mean Hounsfield units (HU) obtained from the arbitrary regions defined over the CT images. The density was calculated based on the relationship [4] between HU, density of the given medium (ρ), and water density (ρ_w) as follows:

$$H = 1000 \left[(\rho / \rho_w) - 1.0 \right]$$

Measurement of Isodose Depths in Different Media

The plans were generated based on the CT images of 10 actual patients, SP34 slab phantom, and SWS phantom. Figure 2 displays the isodose depth patterns in the CT image of one of the actual patients. Figures 3 and 4 illustrate these patterns in SP34 slab and SWS phantoms, respectively. The source to surface distance (SSD) was kept 100 cm in all the plans. All plans involved photon beam of 6 MV with field size of 7.5×7.5 cm^2 irradiated perpendicularly. Dose calculation was performed using the anisotropic analytical algorithm (AAA), version 8.9.08, with the grid size of 0.25 cm. The depths of 100%, 95%, 90%, 85%, 80%, 70%, 60%, and 50% isodose lines were measured on the CT images of 10 patients, SP34 slab phantom, and SWS phantom.

Figure 2. Isodose curves and their depths in CT slice of actual patient
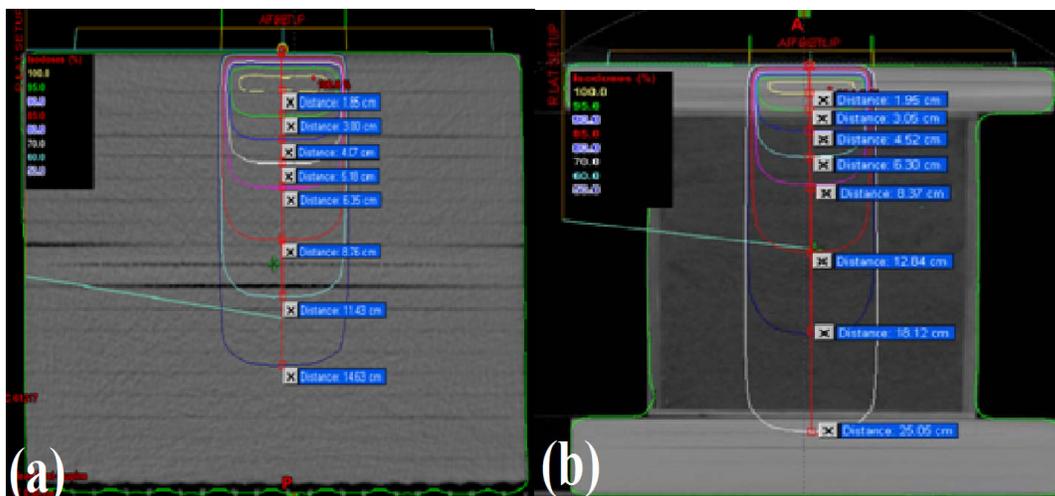
Figure 3. (a) Isodose curves and their depths in CT slice of slab phantom. (b) Isodose curves and their depths in CT slice of WDAS phantom

Point Dose Verification at Different Depths

For the purpose of dose verification in the SP34 slab and SWS phantoms, planning was performed based on the CT images of both phantoms using Eclipse TPS. The plan entailed a single field with 6-MV photon, field size of 7.5×7.5 cm², and SSD of 100 cm. Doses were measured at depths of 2, 13, and 21 cm in TPS for both of the phantoms. All plans were approved on TPS and scheduled to be delivered through Linear accelerator Varian Clinac DMX (Varian Medical Systems, Palo Alto, CA). The phantom was set on Clinac couch.

The ion chamber position was verified by taking kV-cone beam computed tomography images and matching them with primary CT images obtained by means of the Eclipse TPS following the standard imaging procedure [22]. The plan created for each phantom was delivered, and doses were measured at respective depths of 2, 13, and 21 cm using ion chamber (0.13 cc) connected to the DOSE-1 electrometer (IBA Dosimetry, Germany). The planned and measured doses were then compared and analyzed.

Patient-specific quality assurance

Patient-specific QA was performed for intensity modulated radiotherapy (IMRT) plans of 15 randomly selected post mastectomy breast cancer patients. The prescribed dose was 50 Gy in 25 fractions (at the rate of 2 Gy per fraction) with 5 fractions a week. The QA plans were generated on

TPS keeping gantry, couch, and collimator angles zero on SP34 slab and SWS phantoms. Dose was calculated by using AAA with the grid size of 0.25 cm.

Subsequently, the approved plans were transferred to Clinac DMX accelerator. The plans were exposed on SP34 slabs and SWS phantoms. Doses were measured in both of the phantoms by using 0.13 cc ion chamber and DOSE1 electrometer. The percentage variations between the planned and measured doses were calculated using the following formula:

Percentage variation=| (measured dose–planned dose) |/ planned dose×100

Results

The mean densities of wooden dust, SP34 slab phantom, soft tissue, chest wall, and lung are shown in Table 1. Furthermore, the mean depths of 100%, 95%, 90%, 85%, 80%, 70%, 60%, and 50% isodose lines in the thoracic region of 10 actual patients, SP34 slab phantom, and SWS phantom are presented in Table 2. Table 3 illustrates the percentage variation between the planned and measured doses at the depths of 2, 13 and 21 cm in the SP34 slab and SWS phantoms. Additionally, the mean percentage variations between the planned and measured doses for all IMRT QA plans in the SP34 slab and SWS phantoms are displayed in Table 4.

Table 1. Hounsfield unit (HU) and physical density measurement of wooden dust, SP34 slab, soft tissue, chest wall and lung

No of points in given medium	HU of wooden dust	HU of SP34 slab phantom	HU of soft tissue	HU of chest wall	HU of lung
1	-730	-35	-24	-73	-684
2	-750	5	-29	36	-690
3	-733	10	-95	-123	-672
4	-720	-16	-2	-120	-740
5	-713	12	67	-98	-673
6	-739	-11	76	-117	-723
7	-708	11	-70	-28	-714
8	-721	4	-108	-102	-703
9	-748	-20	-75	-111	-699
10	-722	-15	-55	54	-720
11	-733	-19	-108	47	-680
12	-732	9	72	8	-689
13	-735	11	42	-45	-742
14	-717	14	-81	-63	-698
15	-723	2	-43	-91	-726
16	-712	13	-58	-72	-716
17	-716	-38	66	-87	-797
18	-720	-4	-37	-41	-787
19	-744	-8	35	-75	-718
20	-756	-36	20	43	-700
Mean HU	-728.6	-5.55	-20.35	-52.9	-713.55
Density (g/cc)	0.27	0.99	0.98	0.95	0.29

HU: Hounsfield unit

Table 2. Isodose depths in CT images of actual patient, SP34 slab phantom and WDAS phantom

Isodose lines	Mean Isodose depth in patient (cm)	Isodose depth in SP34 slab phantom (cm)	Isodose depth in WDAS phantom (cm)
100%	1.93	1.85	1.95
95%	3.09	3.00	3.05
90%	4.49	4.07	4.52
85%	6.69	5.18	6.30
80%	9.00	6.35	8.37
70%	13.20	8.76	12.84
60%	17.89	11.43	18.12
50%	23.12	14.63	25.05

WDAS phantom: SP34 slab -wooden dust (pine) - SP34 slab

Table 3. Dose at different depths in CT images of actual patient, SP34 slab phantom and WDAS phantom

Depth in cm	Dose in SP34 slab phantom			Dose in WDAS phantom		
	Planned dose(cGy)	Measured dose(cGy)	Percentage variation	Planned dose(cGy)	Measured dose(cGy)	Percentage variation
2	199	199.60	0.30	198.3	198.91	+0.30
13	111.9	110.8	-0.98	138.7	134.30	-3.17
21	70.4	71.	0.85	111.8	108.01	-3.0

cGy: Centi gray; WDAS phantom: SP34 slab -wooden dust (pine) - SP34 slab

Table 4. Percentage variation between planned doses on TPS and measured doses on Clinac using SP34 slab phantom and WDAS phantom

Plan No.	QA plan done on Slab phantom			QA plan done on WDAS phantom		
	Planned dose (cGy)	Measured dose(cGy)	Percentage variation	Planned dose(cGy)	Measured dose(cGy)	Percentage variation
1	175.8	174.75	-1.05	215.6	207.64	-3.69
2	176.46	176.02	-0.44	215.4	208.5	-3.2
3	182.1	180.75	-0.74	230.1	225.23	-2.12
4	209.7	208.49	-1.21	252.6	244.49	-3.21
5	153.5	154.25	0.49	183.3	188.08	2.61
6	163.4	164.9	0.92	158.5	161.9	2.14
7	179.4	181.2	1	177.3	173.7	-2.03
8	202.5	200.8	-0.84	155.7	150.2	-3.53
9	166.6	164.1	-1.5	168.3	172.6	2.55
10	178.5	176.81	-1.69	195.5	190	-2.81
11	192.7	190.2	-1.3	178.3	173.7	-2.58
12	185.9	188.1	1.18	202.8	198	-2.37
13	200.3	202	0.85	188.6	194.9	3.34
14	156	157.3	0.83	165.8	160.3	-3.32
15	193.4	192	-0.72	198.5	191.6	-3.48
Mean			0.98			2.86
SD			0.35			0.56

TPS: treatment planning system; medical linear accelerator (Clinac); QA: quality assurance; cGy: Centi gray; SD: Standard deviation

Discussion

The aim of this study was to find a new material, which can be equivalent to human lung and be used in designing a thorax phantom. To this end, the density and isodepth profiles of this material were studied and compared with those of SP34 slab phantom and actual thorax of 10 patients. According to the literature, the density of the lung varies between 0.2 and 0.5 gm/cc during inhalation and exhalation, respectively [23].

As shown in Table 1, the mean density of the wooden dust (pine) measured in the current study was 0.27 gm/cc, which lies between the density range of an actual human lung. The mean density of SP34 slab phantom was 0.99 gm/cc, which is tissue equivalent and cannot be used to represent the lung while designing thorax phantom for QA purpose.

The actual thorax region of adult male patients includes the chest wall of ~3 cm, lung of ~16 cm, and soft tissue region of ~5 cm. Thorax region acts as a heterogeneous region, where the mean densities of the chest wall, lung, and soft tissue were 0.95, 0.29, and 0.98 gm/cc. When photon beam enters into the chest wall inside the actual patient, it passes through the high-density region of the chest wall; as a result, the attenuation inside the 3-cm chest wall region is higher and the depths of the corresponding isodose lines in this region is lower.

Once the beam enters inside the lung region of ~16 cm depth, it has lower attenuation due to its lower density; therefore, the corresponding isodose lines have higher depths in this region. The soft tissue region has a higher density as compared to the lung; therefore, in the ~5-cm region, the attenuation of beam would increase, and the depths of the corresponding isodose lines would decrease as illustrated in Figure 2.

In the SP34 slab phantom, the density remained constant; therefore, it acted as a medium of uniform density. When photon beam entered to this phantom, the depth of the corresponding isodose lines gradually decreased as shown in Figure 3 (a). This indicated that SP34 slab phantom did not follow the isodose depth pattern of the actual patients. This discrepancy can be due to the fact that the actual patient acts as heterogeneous medium whereas the SP34 slab phantom has a homogeneous density throughout its volume.

The depth of corresponding isodose in the SWS phantom followed the same pattern as that of the actual thorax. As displayed in Figure 3 (b), a 3-cm region in the SWS phantom consisted of slabs with the mean density of 0.99 gm/cc, which resembled to the chest wall of thorax region having the mean density of 0.95 gm/cc. The wooden dust inside the box of 20 cm length with the mean density of 0.27 gm/cc was similar to the lung inside the thorax region having the mean density of 0.29 gm/cc. The slabs of 5 cm thickness with the mean density of 0.99 gm/cc resembled to the soft tissue region behind the lung with the mean density of 0.98 gm/cc.

Therefore, the SWS phantom followed the same density pattern as that of the actual thorax in the patient. This phantom had almost similar depths of corresponding isodose lines to those of the actual thorax as compared to the slab phantom. Variation in the isodose depths between the actual patient and SWS phantom was slightly higher for 50%, 60%, and 70% isodose lines as compared to those for the 80%, 85%, 90%, 95%, 100% isodose lines.

This can be due to the fact that the length of the actual lung was ~16 cm, whereas the wooden box representing the lung in the SWS phantom had a length of 20 cm. Therefore, the density pattern differed in the region within 16-20 cm in patient and SWS phantom. Accordingly, the depths of the corresponding isodoses (i.e., 50%, 60%, and 70% isodose lines), which lie within 16-20 cm slightly varied.

Doses were measured at the depths of 2, 13, and 21 cm in the SP34 slab and SWS phantoms. The phantoms had the same dose at the depth of 2 cm due to having the same density of 0.99 gm/cc and equal attenuation of the photon beam. In the region laying within 3-23 cm of the wooden dust in the SWS phantom, the density was 0.27 gm/cc, whereas SP34 slab phantom had a uniform density of 0.99 gm/cc. The SWS phantom had a greater dose at the depth of 13 cm, compared to the SP34 slab phantom, because the photon beam attenuation was higher in the SP34 slab phantom due to its higher density. Therefore, dose would be lower at higher depths.

The dose measured at 21-cm depth was also higher in the SWS phantom as compared to that in the SP34 slab phantom due to a similar reason. Based on Table 3, percentage variations between the planned doses on the CT images of both phantoms by TPS and measured dose on the Linac accelerator at the depths of 2, 13, and 21 cm were lower in the SP34 slab phantom as compared to those in the SWS phantom.

The reason for observing higher variations in the SWS phantom was due to the use of AAA. The AAA does not calculate doses in a heterogeneous medium as accurately as the MC-based algorithms, such as AXB [24, 25]. Therefore, in case of the SWS phantom, the variation between the measured dose and planned dose on TPS was higher as it is a heterogeneous medium. Since the SWS phantom represented the thorax density pattern of actual patients, AAA would not be efficient for the calculation of dose where the inhomogeneities were involved near boundaries.

The patient-specific QA was performed for IMRT in the breast cancer patients. The variation between the measured dose and the dose calculated by TPS

was lower in the SP34 slab phantom in comparison to that in the SWS phantom. The mean dose variations were lower than 1% and higher than 2% in the SP34 slab and SWS phantoms, respectively. Consequently, this value was within the tolerance limit of 3% in both phantoms [10]. The dose calculation through AAA would result in a higher variation as this algorithm does not efficiently calculate dose with density variation across the heterogeneous boundaries. Therefore, this algorithm would show higher variations in the SWS phantom.

In the present study, all calculations were performed by using AAA since the MC-based algorithms were not available in our TPS during the study period. Therefore, future studies are recommended to use the third-generation MC code-based algorithms for obtaining accurate calculations. The present study highlighted the need for an accurate dose calculation algorithm. In addition, it was suggested that instead of using a homogenous slab phantom for performing patient-specific IMRT QA, we should use a heterogeneous phantom, which mimics the actual thoracic region of the patients.

The current study targeted toward developing an equivalent phantom, which would represent the actual thoracic region of human. Accordingly, in this study, the radiological equivalence of the materials that could be used in fabricating the chest phantom was investigated. The results of the study indicated that the mentioned materials could be utilized in the fabrication of the chest phantom. As the subject under study was a unique concept and no one has used wooden dust or similar kind of material as a lung substitute yet, the results obtained in this study could not be compared with those of other studies.

Conclusion

As the findings of the present study indicated, the density and isodose depth profiles of the SWS phantom were equivalent to those of the actual thoracic region of human. Therefore, the current study could be further explored to develop a thorax phantom, which can replicate the actual thoracic region of human in all aspects. The implementation of patient-specific IMRT QA on such a phantom would definitely improve the patient-specific QA practices as compared to the use of the slab phantom.

Acknowledgment

References

1. Attix FH. Introduction to radiological physics and radiation dosimetry. 1st ed. Hoboken: John Wiley and Sons; Printed in the Federal Republic of Germany. 1986:142-54.
2. Broerse JJ, Zoetelief J. Dose inhomogeneities for photons and neutrons near interfaces. Radiat Prot Dosimetry. 2004; 112(4): 509-17.
3. Ueki N, Matsuo Y, Shibuya K, Nakamura M, Narabayashi M, Sakanaka K, et al. Differences in the dose-volume metrics with heterogeneity correction status and its influence on local control in stereotactic body radiation therapy for lung cancer. J Radiat Res. 2013;54(2):337-43.
4. Gurjar OP, Mishra SP, Bhandari V, Pathak P, Patel P, Shrivastav G. Radiation dose verification using real tissue phantom in modern radiotherapy techniques. J Med Phys . 2014; 39(1): 44-9.
5. Chen WZ, Xiao Y, Li J. Impact of dose calculation algorithm on radiation therapy. World J Radiol. 2014; 6(11): 874-80.
6. Khan FM. The Physics of Radiation Therapy. 5th ed. Baltimore. MD. USA: Lippincott Williams and Wilkins. 2014; 425-28.
7. Gray A, Oliver LD, Johnston PN. The accuracy of the pencil beam convolution and anisotropic analytical algorithms in predicting the dose effects due to attenuation from immobilization devices and large air gaps. Med Phys. 2009; 36(7): 3181–91.
8. Kan MW, Cheung JY, Leung LH, Lau BM, Yu PK. The accuracy of dose calculations by anisotropic analytical algorithms for stereotactic radiotherapy in nasopharyngeal carcinoma. Phys Med Biol. 2011; 56(1): 397–413.
9. Oyewale S. Dose prediction accuracy of collapsed cone convolution superposition algorithm in a multi- layer inhomogeneous phantom. Int J Cancer Ther Oncol. 2013; 1(1): 1-16.
10. Papanikolaou N, Battista J, Mackie T, Kappas C, Boyer A. Tissue inhomogeneity corrections for megavoltage photon beams. AAPM Report No 85; Task Group No. 65, 2004.
11. Fogliata A, Vanetti E, Albers D, Brink C, Clivio A, Knoos T, et al. On the dosimetric behavior of photon dose calculation algorithms in the presence of simple geometric heterogeneities: comparison with Monte Carlo calculations. Phys Med Biol. 2007; 52(5): 1363–85.
12. Ulmer W, Pyyry J, Kaissl W. A 3D photon superposition/ convolution algorithm and its foundation on results of Monte Carlo calculations. Phys Med Biol. 2005;50(8): 1767–90.
13. Fippel M, Haryanto F, Dohm O, Nüsslin F, Kriesen S. A virtual photon energy fluence model for Monte Carlo dose calculation. Med Phys. 2003;30(3):301–11.
14. ICRU Report 83. Prescribing, recording, and reporting photon-beam Intensity-Modulated Radiation Therapy (IMRT). International Commission on Radiation Units and Measurements. (Bethesda, 2010).
15. Watson PE, Watson ID, Batt RD. Total body water volumes for adult males and females estimated from

simple anthropometric measurements. Am J Clin Nutr. 1980; 33(1): 27-39.

16. Absorbed dose determination in external beam radiotherapy: An international code of practice for dosimetry based on absorbed dose to water. IAEA. Vienna; 2000.

17. Low DA, Moran JM, Dempsey JF, Dong L, Oldham M. Dosimetry tools and techniques for IMRT. Med Phys. 2011; 38(3): 1313-38.

18. Kleck JH, Smathers JB, Holly FE, Myers LT. Anthropomorphic radiation therapy phantoms: a quantitative assessment of tissue substitutes. Med Phys. 1990; 17(5): 800–6.

19. Opp D, Nelms BE, Zhang G, Stevens C, and Feygelman V. Validation of measurement-guided 3D VMAT dose reconstruction on a heterogeneous anthropomorphic phantom. J Appl Clin Med Phys. 2013; 14(4): 70-84.

20. Nishio T, Shirato H, Ishikawa M, Miyabe Y, Kito S, Narita Y, et al. Design, development of water tank-type lung phantom and dosimetric verification in institutions participating in a phase I study of stereotactic body radiation therapy in patients with T2N0M0 non-small cell lung cancer: Japan Clinical Oncology Group trial (JCOG0702). J Radiat Res. 2014; 55(3): 600-7.

21. Chang J , Suh TS, Lee DS. Development of a deformable lung phantom for the evaluation of deformable registration. J Appl Clin Med Phys. 2010; 11(1): 281-86.

22. Gurjar OP, Mutneja A, Bagdare P, Bhandari V, Gupta KL, Goyal H, et al. Comparative evaluation of Cone Beam Computed Tomography (CBCT) and Orthogonal Portal Imaging (OPI) in implementation of IMRT protocol in Prostate Cancer. Int J Cancer Ther Oncol. 2016; 4(1): 1-6.

23. Ravikumar B, Lakshminarayana S. Determination of the tissue inhomogeneity correction in high dose rate brachytherapy for iridium‑192 source. J Med Phys. 2012; 37(1): 27‑31.

24. Robinson D. Inhomogeneity correction and the analytic anisotropic algorithm. J Appl Clin Med Phys. 2008; 9(2): 112-22.

25. Rana SB. Dose prediction accuracy of anisotropic analytical algorithm and pencil beam convolution algorithm beyond high density heterogeneity interface. South Asian J Cancer . 2013; 2(1): 26-30.